Interaction Analysis and Posture Optimization for a Reconfigurable Tracked Mobile Modular Manipulator Negotiating Slopes

Yugang Liu and Guangjun Liu, *Senior Member, IEEE*

Abstract— This paper analyzes track-terrain and vehicle-manipulator interactions and develops posture optimization algorithms for a reconfigurable tracked mobile modular manipulator negotiating slopes. A tracked mobile robot is associated with unavoidable slippage due to the fact that there are infinite number of contact points between the tracks and the terrain. Furthermore, the reconfiguration of the tracked mobile robot, motion of the onboard manipulator, as well as the centrifugal forces give rise to transfer of load distribution, complicating track-terrain interactions. For a tracked mobile manipulator negotiating slopes, posture optimization is essential for enhancing the traction performance, improving the efficiency of power consumption and avoiding tip-over instabilities. In this paper, track-terrain and vehicle-manipulator interactions are analyzed for a reconfigurable tracked mobile modular manipulator negotiating slopes, and a real-time posture optimization algorithm is developed by online reconfiguring the tracked mobile platform or adjusting motion of the onboard manipulator. The effectiveness of the developed algorithms has been verified by simulations and experiments.

I. INTRODUCTION

Tracked vehicles have attracted attention from numerous researchers for many years since they have substantial potential applications, such as searching, rescuing, explosive ordnance disposing (EOD), mining, logging, farming, earth moving and planetary exploring, among others. Tracked vehicles normally provide better floatation and traction than wheeled ones because they have larger contact area, which makes them suitable for off-road terrains. However, this characteristic also makes slippage unavoidable, which increases the complexity of track-terrain interactions.

With the introduction of modular concept to tracked mobile robot design, modern self-reconfigurable tracked mobile robots have been endowed with extraordinary locomotion capabilities, such as climbing stairs [1], surpassing obstacles, or negotiating slopes [2]. However, the manipulation potential of a tracked mobile robot is quite limited [3]. To address this issue, the integration with an onboard manipulator provides a promising solution [4], [5], which increases the workspace and scope of applications of the mobile robot and the conventional manipulator dramatically. However, this integration introduces complicated vehicle-manipulator interactions [4].

In related research, irregular terrain has posted a great challenge to mobile robots, and tip-over stability as well as traction optimization for mobile robots traversing irregular

terrain has been paid much attention [6]–[10]. As one of the most omnipresent terrain, slope climbing capability is required for robots to operate efficiently in unstructured environments [2]. The mechanics of vehicle-terrain interaction, which is known as terramechanics, used to be a hot research topic, and steerability analysis has attracted numerous researchers [11]. The conventional dead-reckoning systems, which use wheel encoders and odometry to estimate the linear displacements, have been realized to be unreliable for mobile robots traveling on irregular terrains, and extensive efforts have been made for slip estimation and compensation, as well as odometry correction of off-road mobile robots [12], [13]. Kinematics modeling, track-terrain or wheel-terrain interaction analysis, as well as online pose estimation for mobile robots, have attracted extensive research attention [4], [14], [15]. As non-skidding and non-slipping assumptions have been identified to be impractical for off-road mobile robots, skid-steering control of mobile robots with consideration of tire-terrain interactions have become a research focus [16]–[18].

While tracked vehicles and wheeled mobile manipulators have been extensively studied, only a few works have been reported on tracked mobile manipulators [4], and even less on reconfigurable tracked mobile modular manipulators (RTMMM) [2]. A RTMMM integrates a self-reconfigurable tracked mobile platform with an onboard modular manipulator. The former has strong locomotion capabilities, and the latter can perform sophisticated manipulation tasks in unstructured environments. By reconfiguring the tracked mobile platform or adjusting motion of the onboard manipulator, the load distribution can be optimized so as to enhance the traction performance, to improve tip-over stabilities, and to minimize the consumption of power, which is believed to be one of the most precious commodity for off-road mobile robots. This paper analyzes the track-terrain and vehicle-manipulator interactions for a RTMMM negotiating rigid slopes, on which the sinkage of the tracks is assumed to be negligible. Furthermore, a real-time posture optimization algorithm is developed on the basis of mobile robot reconfiguration or onboard manipulator adjustment.

The rest of this paper is organized as follows: a RTMMM is introduced; the coordinate systems are defined and some necessary assumptions are made in the following section. Slippage and track-terrain, vehicle-manipulator interactions are analyzed in Section III. A real-time posture optimization algorithm is developed in Section IV. Simulation and experimental results are presented in Section V. Some concluding remarks are given in the last section.
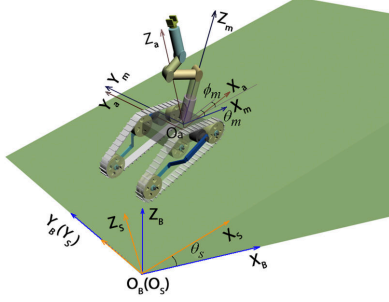
Fig. 1. Coordinates definition for a RTMMM negotiating a slope.

II. COORDINATES DEFINITION AND ASSUMPTIONS

The RTMMM under study is composed of a self-reconfigurable tracked mobile robot called Ryerson Linkage Mechanism Actuator (RLMA), which is a customized product of Engineering Service Inc. (ESI) [19], and an onboard manually reconfigurable modular manipulator, as shown in Fig. 1. For details of the RTMMM, please refer to the authors' previous published papers [1]–[4].

To study the motion of the aforementioned robot negotiating a slope, four coordinate systems are defined as follows: an inertial base frame O_B-$X_BY_BZ_B$ is fixed at the foot of the slope; O_S-$X_SY_SZ_S$ is a frame on the slope; a frame O_m-$X_mY_mZ_m$ is mounted on the tracked vehicle, and an auxiliary frame O_a-$X_aY_aZ_a$ is defined as shown in Fig. 1. Then, the motion of the tracked mobile platform on the slope can be determined by the position $(^sx_m, ^sy_m, ^sz_m)$, the pitch angle θ_m and the yaw angle ϕ_m.

From Fig. 1, the transformation matrices between different frames can be calculated as follows:

$$
{}_S^B\mathbf{T} = \begin{bmatrix} \mathbf{R}_{Y_B}(-\theta_s) & \mathbf{0}_{3\times 1} \\ \mathbf{0}_{1\times 3} & 1 \end{bmatrix}, \quad {}_a^S\mathbf{T} = \begin{bmatrix} \mathbf{R}_{Z_S}(\phi_m) & {}^s\mathbf{p}_a \\ \mathbf{0}_{1\times 3} & 1 \end{bmatrix},
$$
$$
{}_m^a\mathbf{T} = \begin{bmatrix} \mathbf{R}_{Y_a}(-\theta_m) & {}^a\mathbf{p}_m \\ \mathbf{0}_{1\times 3} & 1 \end{bmatrix}
$$

(1)

where $\mathbf{R}_{Y_B}$, $\mathbf{R}_{Z_S}$ and $\mathbf{R}_{Y_a}$ are rotational matrices; $\mathbf{0}_{3\times 1}$ and $\mathbf{0}_{1\times 3}$ denote zero vectors; ${}^s\mathbf{p}_a = [{}^sx_m \quad {}^sy_m \quad r + h_g]^T$ represents coordinates of O_m with respect to O_S-$X_SY_SZ_S$; ${}^a\mathbf{p}_m = [0 \quad 0 \quad {}^az_m]^T$ with ${}^az_m = |O_mO_a|$.

To simplify the calculations, we make the following assumptions: the tracked mobile robot is assumed to be laterally symmetrical, and the onboard manipulator is assumed to situate above the center of gravity (COG) of the chassis; the lateral slippage of the left and right tracks is assumed to be consistent; it is assumed that the track extension can be retained and there is no slippage between the tracks and wheels; moreover, the terrain is assumed to be hard enough so that the sinkage of the tracks can be neglected; furthermore, the track-terrain interactive forces are assumed to be generated immediately under the wheels. Detailed discussions on these assumptions can be found in the authors' previous published papers [2]–[4].

III. SLIP VELOCITIES AND INTERACTION ANALYSIS

In this section, slip velocities of the concerned track-terrain contact points are derived for different configurations. And track-terrain as well as vehicle-manipulator interactive forces are analyzed on the basis of load transfer. With the assumption that the interactive forces are generated immediately under the wheels, six track-terrain contact points are of concern in *Cfg 1*, namely P_{ld}, P_{rd}, P_{ls}, P_{rs}, P_{lp} and P_{rp}. The subscripts 'l' and 'r' denote the left and right track, and 'd', 's', 'p' represent the driving, supporting and planetary wheels, respectively. Since the frame O_a-$X_aY_aZ_a$ overlaps O_m-$X_mY_mZ_m$ in *Cfgs 1–2*, the slip velocities for the concerned track-terrain contact points can be derived by:

$$
\begin{aligned}
\dot{s}_{l\diamond}^x &= \cos\phi_m \, {}^s\dot{x}_m + \sin\phi_m \, {}^s\dot{y}_m - \tfrac{d_m}{2}\dot{\phi}_m - r\,\dot{q}_l \\
\dot{s}_{r\diamond}^x &= \cos\phi_m \, {}^s\dot{x}_m + \sin\phi_m \, {}^s\dot{y}_m + \tfrac{d_m}{2}\dot{\phi}_m - r\,\dot{q}_r \\
\dot{s}_{\star d}^y &= \cos\phi_m \, {}^s\dot{y}_m - \sin\phi_m \, {}^s\dot{x}_m - \left(\tfrac{L}{2}+l_G\right)\dot{\phi}_m \\
\dot{s}_{\star s}^y &= \cos\phi_m \, {}^s\dot{y}_m - \sin\phi_m \, {}^s\dot{x}_m + \left(\tfrac{L}{2}-l_G\right)\dot{\phi}_m \\
\dot{s}_{\star p}^y &= \cos\phi_m \, {}^s\dot{y}_m - \sin\phi_m \, {}^s\dot{x}_m + [\pm L_p(0)-l_G]\dot{\phi}_m
\end{aligned}
$$

(2)

where $\star \in \{l, r\}$; $\diamond \in \{d, s, p\}$ for *Cfg 1* and $\diamond \in \{d, s\}$ for *Cfg 2*; the last equation in (2) does not apply to *Cfg 2*, and '+','−' correspond to $\theta_p = 0$, $\theta_p = \pi$ of *Cfg 1*, respectively. Details on the derivation can be found in [4].

Regarding *Cfg 3*, the concerned track-terrain contact points are denoted as P_{ls}, P_{rs}, P_{lp} and P_{rp}. From Fig. 2(e), we can obtain the slip velocities for *Cfg 3*, as follows:

$$
\begin{aligned}
\dot{s}_{l\diamond}^x &= \cos\phi_m \, {}^s\dot{x}_m + \sin\phi_m \, {}^s\dot{y}_m - \tfrac{d_m}{2}\dot{\phi}_m \\
&\quad - \left(\tfrac{L}{2}-l_G\right)\cos\phi_m\sin\theta_m\,\dot{\theta}_m - r\,\dot{q}_l \\
\dot{s}_{r\diamond}^x &= \cos\phi_m \, {}^s\dot{x}_m + \sin\phi_m \, {}^s\dot{y}_m + \tfrac{d_m}{2}\dot{\phi}_m \\
&\quad - \left(\tfrac{L}{2}-l_G\right)\cos\phi_m\sin\theta_m\,\dot{\theta}_m - r\,\dot{q}_r \\
\dot{s}_{\star s}^y &= \cos\phi_m \, {}^s\dot{y}_m - \sin\phi_m \, {}^s\dot{x}_m + \left(\tfrac{L}{2}-l_G\right) \\
&\quad \cdot \left[\cos\theta_m\,\dot{\phi}_m + \sin\phi_m\sin\theta_m\,\dot{\theta}_m\right] \\
\dot{s}_{\star p}^y &= \cos\phi_m \, {}^s\dot{y}_m - \sin\phi_m \, {}^s\dot{x}_m + \left(\tfrac{L}{2}-l_G\right)\sin\phi_m \\
&\quad \cdot \sin\theta_m\,\dot{\theta}_m - [l_G\cos\theta_m - L_p\cos(\theta_p+\theta_m)]\dot{\phi}_m
\end{aligned}
$$

(3)

Similarly, we can obtain the slip velocities for the concerned track-terrain contact points of *Cfg 4*: P_{ld}, P_{rd}, P_{lp} and P_{rp}, which have the similar form as shown in (3), but replacing $\tfrac{L}{2}-l_G$ with $-\left(\tfrac{L}{2}+l_G\right)$.

For the convenience of presentation, the masses for all the parts of the robot are simplified to an equivalent COG, as shown in Fig. 2. Furthermore, to simplify the calculations, the external force vector $\mathbf{f}_{ext}$ and the gravity acceleration vector $\mathbf{g}$ are projected to frames O_S-$O_SX_SY_SZ_S$ and O_a-$X_aY_aZ_a$ as ${}^s\mathbf{f}_{ext}$, ${}^a\mathbf{f}_{ext}$, ${}^s\mathbf{g}$, ${}^a\mathbf{g}$, respectively.

For the convenience of posture optimization, the normal forces with respect to frame O_S-$X_SY_SZ_S$ are derived based on load transfer and are decomposed into three parts as:

$$
N_{\star\diamond} = \bar{N}_{\star\diamond} + \delta N_{\star\diamond}^x + \delta N_{\star\diamond}^y \tag{4}
$$

where $\bar{N}_{\star\diamond}$ is the normal force in the static condition under which the gravity is assumed to be concentrated in the geometry center of the track-terrain contact area, and the

accelerations, the inertial forces, as well as the external forces are all assumed to be zero. $\delta N_{\star\diamond}^x$ and $\delta N_{\star\diamond}^y$ represent the change of normal force caused by longitudinal and lateral load transfer due to the offset of COG, the inertial forces, the centrifugal forces and the external forces.

In *Cfg 1*, if $\theta_p = 0$, assume that the normal forces are distributed along the longitudinal direction in the form of trapezoid [11], from Fig. 2(b), we can obtain

$$\bar{N}_{\star d} = \left(-\tfrac{1}{2}m \cdot {}^a g_z\right)\left\{\frac{L_{p0}^2 + \tfrac{7}{4}L^2}{3L^2 + 4L_{p0}^2}\right\}$$
$$\bar{N}_{\star s} = \left(-\tfrac{1}{2}m \cdot {}^a g_z\right)\left\{\frac{\left(\tfrac{L}{2}+L_{p0}\right)^2}{3L^2 + 4L_{p0}^2}\right\} \quad (5)$$
$$\bar{N}_{\star p} = \left(-\tfrac{1}{2}m \cdot {}^a g_z\right)\left\{\frac{L^2 - LL_{p0} + 2L_{p0}^2}{3L^2 + 4L_{p0}^2}\right\}$$

Furthermore, the longitudinal load transfer can be calculated as follows:

$$\delta N_{\star d}^x = \tfrac{1}{2}\left\{\frac{(m\,{}^a\ddot{z}_G - {}^a F_{ext}^z)\left(L_{p0}^2 + \tfrac{7}{4}L^2\right) + (2L_{p0}+3L)\cdot\delta N^x}{3L^2 + 4L_{p0}^2}\right\}$$
$$\delta N_{\star s}^x = \tfrac{1}{2}\left\{\frac{(m\,{}^a\ddot{z}_G - {}^a F_{ext}^z)\cdot\left(L_{p0}+\tfrac{L}{2}\right)^2 + (2L_{p0}-3L)\cdot\delta N^x}{3L^2 + 4L_{p0}^2}\right\} \quad (6)$$
$$\delta N_{\star p}^x = \tfrac{1}{2}\left\{\frac{(m\,{}^a\ddot{z}_G - {}^a F_{ext}^z)\left(L^2 - LL_{p0} + 2L_{p0}^2\right) - 4L_{p0}\cdot\delta N^x}{3L^2 + 4L_{p0}^2}\right\}$$

where δN^x can be detailed by

$$\delta N^x = m\left({}^a\ddot{x}_G - {}^a\dot{y}_G\dot{\phi}_m + a_{CF}^x - {}^a g_x\right){}^s z_G - {}^a F_{ext}^x\,{}^s z_e$$
$$+ m\left({}^a\ddot{z}_G - {}^a g_z\right)(l_{c1} - {}^a x_G) - {}^a F_{ext}^z(l_{c1} - {}^a x_e) \quad (7)$$

where $l_{c1} = \frac{L_{p0}}{2} - \frac{L}{4} - l_G$, and ${}^a x_e$, ${}^a y_e$, ${}^a z_e$, ${}^s x_e$, ${}^s y_e$, ${}^s z_e$ denote coordinates of the end-effector with respect to O_a-$X_a Y_a Z_a$ and O_S-$X_S Y_S Z_S$, respectively.

With the assumption that lateral load transfer is consistent, from Fig. 2(c), we can obtain the lateral load transfer as:

$$\delta N_{l\diamond}^y = -\delta N_{r\diamond}^y = \frac{m\left({}^a g_y - {}^a\ddot{y}_G - {}^a\dot{x}_G\dot{\phi}_m - a_{CF}^y\right){}^s z_G}{d_m}$$
$$+ \frac{m\left({}^a\ddot{z}_G - {}^a g_z\right){}^a y_G + {}^a F_{ext}^y\,{}^s z_e - {}^a F_{ext}^z\,{}^a y_e}{d_m} \quad (8)$$

Exchanging the subscripts 'd', 's', 'p' with 'p', 'd', 's' in (5–6) and replacing l_{c1} with $l'_{c1} = \frac{L}{4} - \frac{L_{p0}}{2} - l_G$ in (7), we can obtain the longitudinal load transfer for *Cfg 1* on the condition that $\theta_p = \pi$. The lateral load transfer has the same form as shown in (8) when $\theta_p = \pi$, as well as for *Cfgs 2–4*.

In *Cfg 2*, the normal forces in static condition are

$$\bar{N}_{\star\diamond} = -\frac{1}{4}m \cdot {}^a g_z \quad (9)$$

where $\star \in \{l, r\}$ and $\diamond \in \{d, s\}$.

With the assumption that the spring is in its equilibrium length when $\theta_p = 0$, the track tension caused by spring compression of the flippers and that due to longitudinal tractive forces can be calculated from Fig. 2(d) as follows:

$$F_{\star t1} = \frac{k_f \cdot [L_p(0) - L_p(\theta_p)] + m_p \cdot {}^a g_z \cdot \sin\theta_p}{\cos(\theta_p - \theta_r) + \cos(\theta_f - \theta_p)}$$
$$F_{\star t2} = \begin{cases} -\sum\limits_{\diamond\in\{d,s\}} F_{\star\diamond}^x, & \dot{q}_\star < 0 \\ 0, & \dot{q}_\star \geq 0 \end{cases} \quad (10)$$
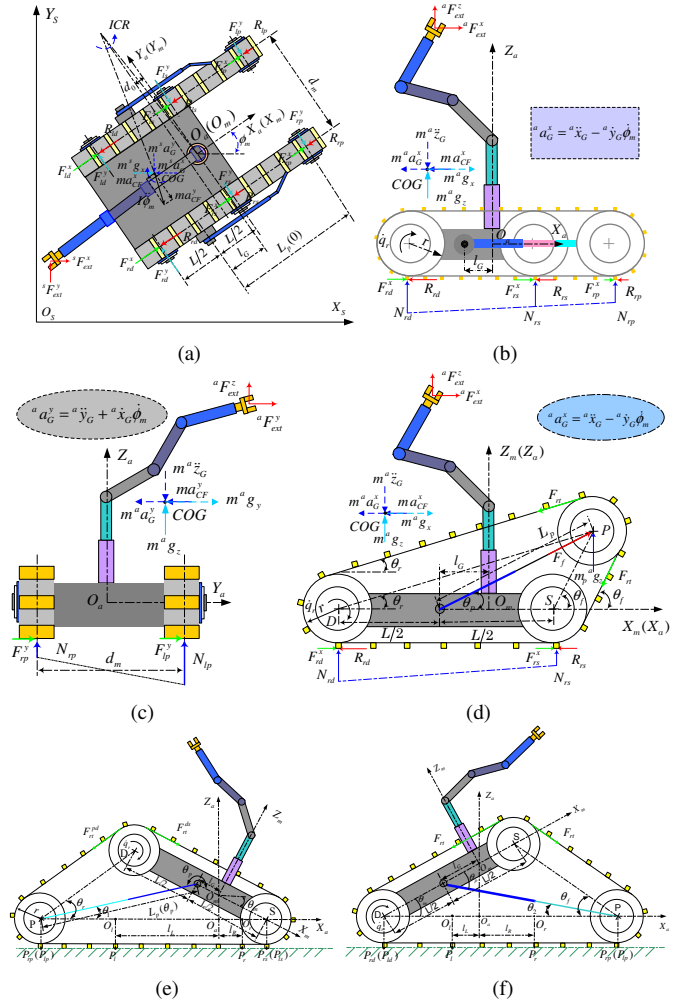

Fig. 2. Interaction analysis for a RTMMM negotiating a slope. (a) View from the direction of $O_s Z_s$: *Cfg 1*. (b) View along $O_m Y_m$:*Cfg 1*. (c) View from the direction of $O_m X_m$: *Cfg 1*. (d) View from the direction of $O_s Z_s$: *Cfg 2*. (e) view along the direction of $O_m Y_m$: *Cfg 3*. (f) View along the direction of $O_m Y_m$: *Cfg 4*.

where k_f is the spring constant of the flippers; θ_f and θ_r are the approach and departure angle of the track, as shown in Fig. 2(d); the tractive forces, assuming that cohesion and adhesion on the track-terrain interface can be considered negligible, can be derived as

$$F_{\star\diamond}^x = \mu_x \cdot N_{\star\diamond} \cdot \left[1 - \exp\left(-\frac{K\cdot|\dot{s}_{\star\diamond}^x|}{max(|\dot{s}_{\star\diamond}^x + r\dot{q}_\star|, |r\dot{q}_\star|)}\right)\right]$$
$$\cdot \cos\left[\pi + \arctan 2\left(\dot{s}_{\star\diamond}^y, \dot{s}_{\star\diamond}^x\right)\right]$$
$$F_{\star\diamond}^y = \mu_y \cdot N_{\star\diamond} \cdot \left[1 - \exp\left(-\frac{K\cdot|\dot{s}_{\star\diamond}^x|}{max(|\dot{s}_{\star\diamond}^x + r\dot{q}_\star|, |r\dot{q}_\star|)}\right)\right]$$
$$\cdot \sin\left[\pi + \arctan 2\left(\dot{s}_{\star\diamond}^y, \dot{s}_{\star\diamond}^x\right)\right] \quad (11)$$

where μ_x and μ_y are the longitudinal and lateral coefficients of friction between the track and the terrain; and K is a coefficient in pull-slip equation [4].

From Fig. 2(d), the longitudinal load transfer for *Cfg 2* can be calculated by

$$\delta N_{\star d}^x = \frac{m\,{}^a\ddot{z}_G - {}^a F_{ext}^z}{4} + \frac{\delta N^x}{2L} + \frac{F_{\star t}(\sin\theta_f - \sin\theta_r)}{2}$$
$$\delta N_{\star s}^x = \frac{m\,{}^a\ddot{z}_G - {}^a F_{ext}^z}{4} - \frac{\delta N^x}{2L} - \frac{F_{\star t}(\sin\theta_f - \sin\theta_r)}{2} \quad (12)$$

where $F_{\star t} = F_{\star t1} + F_{\star t2}$; $\frac{\delta N^x}{2L}$ is the longitudinal load

transfer caused by the inertial forces, the external force, the offset of COG and the centrifugal forces, and δN^x can be obtained from (7) by replacing l_{c1} with $l_{c2} = -l_G$.

With respect to *Cfgs 3–4*, the normal force in the static condition has the same form as shown in (9) but replacing $\diamond \in \{d, s\}$ with $\diamond \in \{s, p\}$ or $\diamond \in \{d, p\}$, respectively. The longitudinal load transfer and lateral load transfer can be calculated in a similar way as that for *Cfg 2*, which will not be detailed to avoid unnecessary duplication.

IV. A REAL-TIME POSTURE OPTIMIZATION ALGORITHM

The traction performance of a RTMMM is directly associated with the interactive forces generated at the concerned track-terrain interactive points. Thus, posture control is a feasible way to enhance the traction performance. Moreover, posture control can also be used to balance the load distribution, so as to improve the tip-over stability [2]. Furthermore, the efficiency of power consumption is relevant to slippage and tractive forces, which can be adjusted by posture control.

Traction optimization for wheeled mobile robots has been investigated and the optimization criterion is normally selected to minimize the maximum ratio of the tractive force to the normal force [7]–[9]. With the assumption that the terrain is isotropic, i.e., $\mu_x = \mu_y = \mu$, from (11), the ratio of tractive force to normal force at a concerned track-terrain contact point can be calculated by

$$\rho_{\star\diamond} = \frac{\sqrt{(F_{\star\diamond}^x)^2 + (F_{\star\diamond}^y)^2}}{N_{\star\diamond}} = \mu\left[1 - \exp\left(-\frac{K \cdot |\dot{s}_{\star\diamond}^x|}{\max(|\dot{s}_{\star\diamond}^x + r\dot{q}_\star|, |r\dot{q}_\star|)}\right)\right] \tag{13}$$

From (13), the traction performance of a tracked mobile robot is determined by the longitudinal slip velocities, which are determined by track-terrain interactive parameters and the motion trajectories. When executing a specific task on a specific terrain, $\rho_{\star\diamond}$ is difficult to adjust for a tracked mobile robot. A new traction optimization criterion is developed in this paper based on the fact that terrain failure is normally caused by the maximum track-terrain interactive force, which may result in gross slippage. Thus, to improve traction performance, the maximum track-terrain interactive force should be minimized. Since the tractive force is proportional to the normal force for a specific task, traction optimization can be realized by minimizing the maximum normal force.

From the tip-over stability analysis in our previous researches [1], [2], the tip-over stability of a tracked mobile robot is determined by the minimum normal force generated at the concerned track-terrain contact points. To avoid tipping overs, the minimum normal force needs to be maximized.

An optimization criterion for minimum power consumption of wheeled mobile robots was proposed in [7], which related the power consumption to tractive force. In the same way, we can estimate the power consumption for driving a tracked mobile robot as follows

$$P_d = \frac{Rr^2}{\gamma^2 K_t^2} \sum_{\star \in \{l,r\}} \sum_{\diamond \in \Omega_\diamond} \left\{ (F_{\star\diamond}^x)^2 + (F_{\star\diamond}^y)^2 \right\} \tag{14}$$

where R is the motor resistance; γ is the motor gear ratio; K_t is the motor torque constant; and $\Omega_\diamond = \{d, s, p\}$ for *Cfg 1*,

$\Omega_\diamond = \{d, s\}$ for *Cfg 2*, $\Omega_\diamond = \{s, p\}$ for *Cfg 3*, $\Omega_\diamond = \{d, p\}$ for *Cfg 4*.

Substituting (13) into (14) yields

$$P_d = \frac{Rr^2}{\gamma^2 K_t^2} \sum_{\star \in \{l,r\}} \sum_{\diamond \in \Omega_\diamond} \left\{ \rho_{\star\diamond}^2 N_{\star\diamond}^2 \right\} \geq \frac{Rr^2}{\gamma^2 K_t^2}$$
$$\cdot \left\{ \rho_{l\diamond}^2 \left(\frac{\sum_{\diamond \in \Omega_\diamond} N_{l\diamond}}{n_\diamond}\right)^2 + \rho_{r\diamond}^2 \left(\frac{\sum_{\diamond \in \Omega_\diamond} N_{r\diamond}}{n_\diamond}\right)^2 \right\} \tag{15}$$

where $n_\diamond = 3$ for *Cfg 1* and $n_\diamond = 2$ for *Cfgs 2–4*; P_d gets the minimum value when the normal force for each track equals with each other.

From the above analysis, traction enhancement requires to minimize the maximum normal force, tip-over avoidance needs to maximize the minimum normal force, and power consumption optimization requests to balance the load distribution along the longitudinal direction. Minimizing the maximum normal force or maximizing the minimum normal force may result in over-adjustment, and the switch of contact points, which generate the maximum or minimum normal force, may lead to discontinuity of the optimization function. One alterative is to minimize the difference between the normal forces generated at the concerned track-terrain contact points, so as to reduce the maximum normal force and increase the minimum one in the mean time, which is also consistent with the requirement of balancing the load distribution. Therefore, an optimization function can be defined by minimizing the load transfer along the longitudinal and lateral directions, as follows

$$\Phi = \sum_{\star \in \{l,r\}} \sum_{\diamond \in \{d,s,p\}} \left\{ \frac{w_1}{2} (\delta N_{\star\diamond}^x)^2 + \frac{w_2}{2} (\delta N_{\star\diamond}^y)^2 \right\} \tag{16}$$

where w_1 and w_2 are constants, and can be adjusted to balance the weight for different optimization criteria.

The optimization function defined above can be minimized by adjusting the onboard manipulator or reconfiguring the tracked mobile platform, i.e.,

$$\begin{aligned} \dot{q}_j &= -k_j \cdot \frac{\partial \Phi}{\partial q_j} & (a) \\ \dot{\theta}_p &= -k_p \cdot \frac{\partial \Phi}{\partial \theta_p} & (b) \end{aligned} \tag{17}$$

where $k_j > 0$ and $k_p > 0$ are constants; $\theta_p \in \{0, \pi\}$ for *Cfg 1*, $\theta_p \in (0, \pi)$ for *Cfg 2*, $\theta_p \in (\pi, \frac{3}{2}\pi)$ for *Cfg 3*; and $\theta_p \in (-\frac{1}{2}\pi, 0)$ for *Cfg 4*; furthermore, for all the cases, the physical limits should not be surpassed, i.e., $q_j \in (q_{jmin}, q_{jmax})$, $\dot{q}_j \in (\dot{q}_{jmin}, \dot{q}_{jmax})$, and $\dot{\theta}_p \in (\dot{\theta}_{pmin}, \dot{\theta}_{pmax})$.

It should be noted that reconfiguring the tracked mobile robot or adjusting motion of the onboard manipulator also need power, which can be calculated by [20]

$$P_c = \dot{\theta}_p \cdot \tau_p + \sum_{j=1}^{n} \{\dot{q}_j \cdot \tau_j\} \tag{18}$$

where P_c is the power consumption for control; τ_p and τ_j represent the control input from the actuators of the pitch motor and the jth joint for the onboard manipulator, respectively. Modeling and control for conventional manipulators are well-documented topics, and will not be detailed here.

TABLE I
DESIGN PARAMETERS FOR THE ROBOT

Parameters	Values	Parameters	Values
L (m)	0.514	$m_m (kg)$	42.00
L_t (m)	2.046	m_0 (kg)	3.000
l_1 (m)	0.200	m_1 (kg)	3.000
l_2 (m)	0.460	m_2 (kg)	3.000
l_3 (m)	0.460	m_3 (kg)	3.000
l_4 (m)	0.300	m_4 (kg)	2.000
l_5 (m)	0.100	m_5 (kg)	1.500
l_0 (m)	0.100	m_p (kg)	1.300
h_0 (m)	0.170	m_f (kg)	1.100
h_g (m)	0.010	r (m)	0.100
l_G (m)	0.200	d_m (m)	0.454

Remark 1: In practical applications, the end-effector may have to follow a specific trajectory to perform sophisticated manipulation tasks. To optimize the posture of the RTMMM, self-motions can be used if the robot is redundant. For details on secondary tasks execution of redundant mobile manipulators, the readers are referred to one of the authors' previous published papers [21].

V. SIMULATION AND EXPERIMENTAL RESULTS

A. Simulation Results

To verify the effectiveness of the developed posture optimization algorithm, simulations are conducted on a reconfigurable tracked mobile modular manipulator, which is composed of the RLMA and a 5-DOF onboard manipulator, as shown in Fig. 1. The design parameters for the robot are listed in Table I. In this simulation, the RLMA is controlled to follow a circle on a slope with the incline angle of $36°$; and the simulation time is selected as $t \in [0, 24]$ s. The joint angles for the onboard manipulator are initialized to be $\mathbf{q}(0) = [0 \ \frac{\pi}{4} \ 0 \ 0]^T$. It should be noted that the last joint in Fig. 1 does not influence the load distribution, and will not be controlled in the simulation.

Simulations are conducted for two different schemes: in *Scheme 1*, the onboard manipulator is locked at the initial configuration. In *Scheme 2*, the onboard manipulator is adjusted according to the posture optimization algorithm given by (17a). The joint limits are assumed to be $q_1 \in [-2\pi, +2\pi]$, and $q_j \in [-\frac{2\pi}{3}, +\frac{2\pi}{3}](j = 2, 3, 4)$; moreover, the joint angular velocity limits are assumed to be $\dot{q}_j \in [-1.5, +1.5]$ rad/s; furthermore, the track-terrain interactive parameters are selected as: $f_r = 0.026$, $K = 13.333$ and $\mu = 0.9$. In addition, the constants in *Scheme 2* are selected as $w_1 = w_2 = 1.0$, $k_j = 10^{-4}(j = 1, 2, \cdots, 5)$.

The simulation results are given by Fig. 3. Figs. 3(a)–(b) represent the calculated normal forces for the two different schemes, which are required to construct a force-balanced system. Fig. 3(c) shows the joint angular velocities for the onboard manipulator in *Scheme 2*. The maximum and the minimum normal forces, as well as the power consumption are compared for two different schemes, as shown in Figs. 3(d)–(f), respectively. In Fig. 3(f), $R = 4.348$ Ohm,
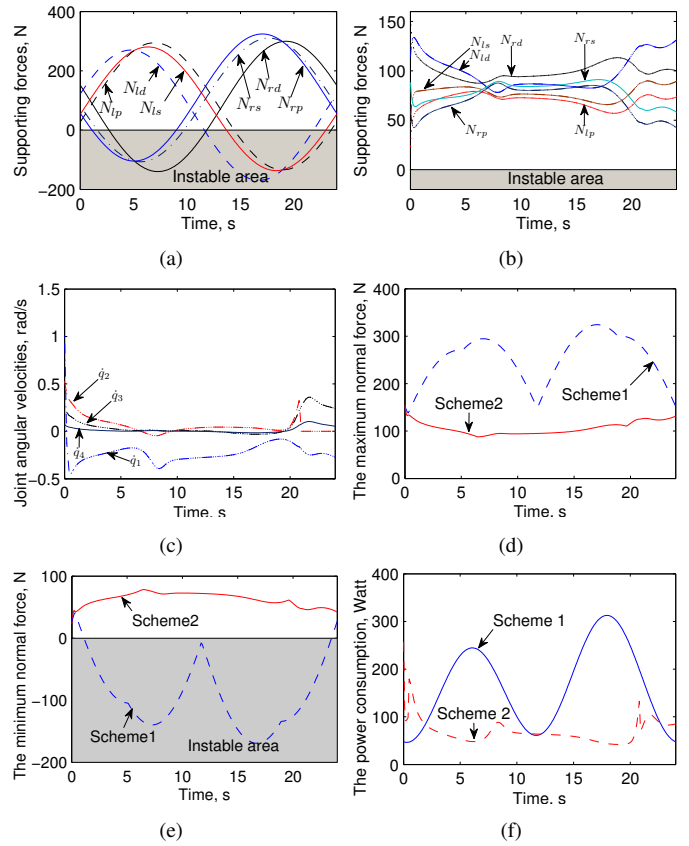
Fig. 3. Simulation results. (a) Calculated normal forces in *Scheme 1*. (b) Calculated normal forces in *Scheme 2*. (c) Joint velocities in *Scheme 2*. (d) Comparison of the maximum normal force. (e) Comparison of the minimum normal force. (f) Comparison of power consumption.
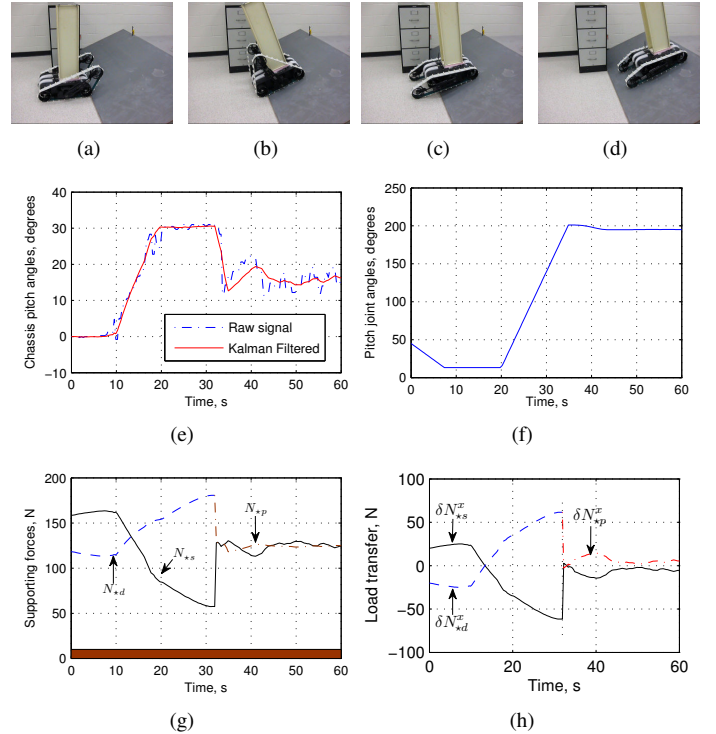
Fig. 4. Experimental results. (a)–(d) Snapshots for the RLMA negotiating a slope. (e) Chassis pitch angles. (f) Pitch joint angles. (g) Calculated normal forces. (h) Load transfers.

$\gamma = 80$ and $K_t = 0.078 \ Nm/Amp$ are used for calculation of the power consumption, which are derived from the specification of the motor and gear head of the RLMA.

From Figs. 3(a)–(b), we can see that the posture optimization algorithm with manipulator adjustment is effective to balance the load distribution among the concerned track-terrain contact points. To avoid surpassing the joint limits, the second joint is locked at about $t = 21.4 \ s$, and the corresponding joint angular velocity is reduced to be zero in the corresponding section of Fig. 3(c); and this also explains why the lateral load transfers increase in such a time interval. From Fig. 3(d), the maximum normal force has been reduced dramatically in *Scheme 2*, which is helpful to reduce the possibility of terrain failure and the resulting gross slippage. In *Scheme 1*, the robot would have tipped over to the left side at about $t = 2 \ s$, since all the required normal forces for the right track have become negative at that moment, as shown in Fig. 3(a). On the other side, the load distribution has been balanced successfully to avoid getting into the instable area with the proposed tip-over avoidance algorithm in *Scheme 2*, as shown in Fig. 3(b). Furthermore, the power consumption has been reduced dramatically with the developed optimization algorithm, as shown in Fig. 3(f).

B. Experimental Results

In the last subsection, the posture optimization algorithm with onboard manipulator adjustment has been verified by simulations. In this subsection, the effectiveness of the proposed posture optimization algorithm are verified through experiments on the RLMA, as shown in Figs. 4(a)–(d).

To simulate the onboard manipulator, a $9.6\text{-}kg$ steel frame is attached to the RLMA, which has the dimension of $25 \times 17 \times 92 \ cm^3$. The experiment is conducted on a $30°$ slope, which is constructed by a steel reenforced plane, and its deformation is negligible. In the experiment, the pitch angles are collected from the compass mounted inside the chassis of the RLMA, which is too noisy to be used for posture optimization. A Kalman filter is used to remove the noises, so as to estimate the pitch angles in the presence of noise.

The experimental results are shown in Figs. 4(e)–(h): the raw chassis pitch angles and the filtered ones are illustrated in Fig. 4(e); the time-varying pitch joint angle is shown in Fig. 4(f); Figs. 4(g)–(h) represent the calculated normal forces and load transfer, respectively. From these figures, we can see that the proposed posture optimization algorithm can be used to balance load distribution by reconfiguring the tracked mobile platform.

VI. CONCLUSIONS

In this paper, track-terrain and vehicle-manipulator interactions have been analyzed and a real-time posture optimization algorithm is developed for a reconfigurable tracked mobile modular manipulator negotiating slopes, in order to enhance the traction performance, to improve the tip-over stability and to minimize the power consumption in the mean time. Slip velocities and interactive forces are analyzed for the reconfigurable tracked mobile modular manipulator with different configurations. Optimization criteria are derived for traction enhancement, tip-over avoidance and power consumption efficiency improvement, and a real-time posture optimization algorithm is developed on the basis of load transfer, which can balance the load distribution by online reconfiguring the tracked mobile platform or adjusting the onboard manipulator. The proposed algorithms have been verified by simulations and experiments.

REFERENCES

[1] Y. Liu and G. Liu, "Track-stair interaction analysis and online tip-over prediction for a self-reconfigurable tracked mobile robot climbing stairs," *IEEE/ASME Trans. on Mechatronics*, vol. 14, no. 5, pp. 528–538, Oct. 2009.

[2] ——, "Interaction analysis and online tip-over avoidance for a reconfigurable tracked mobile modular manipulator negotiating slopes," *IEEE/ASME Trans. on Mechatronics,* in press (DOI: 10.1109/TMECH.2009.2031174), 2010.

[3] ——, "Mobile manipulation using tracks of a tracked mobile robot," in *Proc. IEEE/RSJ Intl. Conf. on Intelligent Robotics and Syst.*, St. Louis, MO, USA, Oct. 2009, pp. 948–953.

[4] ——, "Modeling of tracked mobile manipulators with consideration of track-terrain and vehicle-manipulator interactions," *Robotics and Autonomous Systems*, vol. 57, no. 1, pp. 1065–1074, Nov. 2009.

[5] Y. Li and Y. Liu, "Real-time tip-over prevention and path following control for redundant nonholonomic mobile modular manipulators via fuzzy and neural-fuzzy approaches," *ASME Trans.: J. of Dyn. Syst., Measur., and Contr.*, vol. 128, no. 4, pp. 753–764, Dec 2006.

[6] K. Iagnemma, A. Rzepniewski, S. Dubowsky, and P. Schenker, "Control of robotic vehicles with actively articulated suspensions in rough terrain," *Autonomous Robots*, vol. 14, no. 1, pp. 5–16, Jan. 2003.

[7] K. Iagnemma and S. Dubowsky, "Traction control of wheeled robotic vehicles in rough terrain with application to planetary rovers," *Intl. J. Robot. Res.*, vol. 23, no. 10–11, pp. 1029–1040, Oct.–Nov. 2004.

[8] C. Grand, F. Benamar, F. Plumet, and P. Bidaud, "Stability and traction optimization of a reconfigurable wheel-legged robot," *Intl. J. Robot. Res.*, vol. 23, no. 10–11, pp. 1041–1058, Oct.–Nov. 2004.

[9] S. V. Sreenivasan and B. H. Wilcox, "Stability and traction control of an actively actuated micro-rover," *Journal of Robotic Systems*, vol. 11, no. 6, pp. 487–502, 1994.

[10] A. Diaz-Calderon and A. Kelly, "On-line stability margin and attitude estimation for dynamic articulating mobile robots," *Intl. J. Robot. Res.*, vol. 24, no. 10, pp. 845–866, Oct. 2005.

[11] J. Y. Wong, *Theory of Ground Vehicles*, 4th ed. NJ, USA: John Wiley & Sons Inc., 2008.

[12] C. C. Ward and K. Iagnemma, "A dynamic-model-based wheel slip detector for mobile robots on outdoor terrain," *IEEE Trans. on Robotics*, vol. 24, no. 4, pp. 821–831, Aug. 2008.

[13] K. Iagnemma and C. C. Ward, "Classification-based wheel slip detection and detector fusion for mobile robots on outdoor terrain," *Autonomous Robots*, vol. 26, no. 1, pp. 33–46, Jan. 2009.

[14] J. L. Martinez, A. Mandow, J. Morales, S. Pedraza, and A. Garcia-Cerezo, "Approximating kinematics for tracked mobile robots," *Intl. J. Robot. Res.*, vol. 24, no. 10, pp. 867–878, Oct. 2005.

[15] G. Ishigami, A. Miwa, K. Nagatani, and K. Yoshida, "Terramechanics-based model for steering maneuver of planetary exploration rovers on loose soil," *J. of Field Robot.*, vol. 24, no. 3, pp. 233–250, Mar. 2007.

[16] D. Wang and C. B. Low, "Modeling and analysis of skidding and slipping in wheeled mobile robots: control design perspective," *IEEE Trans. on Robotics*, vol. 24, no. 3, pp. 676–687, June 2008.

[17] C. B. Low and D. Wang, "Gps-based tracking control for a car-like wheeled mobile robot with skidding and slipping," *IEEE/ASME Trans. on Mechatronics*, vol. 13, no. 4, pp. 480–484, Aug. 2008.

[18] J. Yi, D. Song, J. Zhang, and Z. Goodwin, "Adaptive trajectory tracking control of skid-steered mobile robots," in *Proc. of IEEE Intl. Conf. on Robot. and Autom.*, Roma, Italy, Apr. 2007, pp. 2605–2610.

[19] ESI, LMA series of mobile platforms. [Online]. Available: http://www.esit.com/mobileRobots.php

[20] J. J. E. Slotine, "Putting physics in control – the example of robotics," *IEEE Control Syst. Magazine*, vol. 8, no. 6, pp. 12–18, Dec. 1988.

[21] Y. Liu and G. Liu, "On multiple secondary task execution of redundant nonholonomic mobile manipulators," *Journal of Intelligent and Robotic Systems*, vol. 56, no. 4, pp. 365–388, Nov. 2009.